Blocking, gap flow and mountain wave interaction along the coastal escarpment of South Africa

Markus Geldenhuys[1 ab]

Dr Liesl L Dyson [a]

Deon van der Mescht [b]

[a] University of Pretoria, Faculty of Natural and Agricultural Sciences, Department of Geography, Geoinformatics and Meteorology, Lynnwood Road, Pretoria

[b] South African Weather Service, Port Elizabeth Forecasting Office, Allister Miller Drive, Port Elizabeth

Liesl Dyson: ORCID ID: https://orcid.org/0000-0003-2931-8824

Markus Geldenhuys: ORCID ID: https://orcid.org/0000-0001-6273-5633

Declarations of interest: none

Acknowledgements

I, Markus Geldenhuys, would like to express my sincere gratitude to the late Prof J van Heerden for teaching me everything I know about experiment design. I would also like to thank Mr E Engelbrecht for always availing himself during field campaigns and for not complaining when he climbed Africa Peak during 160 km/h winds and -7 °C apparent temperature. I am also indebted to Mr H van Niekerk and the SAWS Eastern Cape forecasting team. This project would not have been possible without your support.

Thank you to InterMet Africa Systems for sponsoring 20 radiosondes and the use of radiosonde equipment, and Air Liquide for sponsoring the hydrogen gas for the balloons. I would also like to thank the South African Weather Service for the time, use of equipment and study bursary.

Abstract

A fatal light aircraft crash occurred in the complex mountainous terrain along the coast of the South African Southern Cape in December 2015. An investigation into the meteorological conditions on this day revealed the interaction between mountain waves, gap flow and blocking near a cold front. The crash highlighted the need to equip forecasters with knowledge of the turbulence produced under these circumstances. With this in mind, experiments were conducted within vicinity of the crash site, with automatic weather stations

Corresponding author: Markus Geldenhuys, Forshchungszentrum Juelich, Institute of Energy and Climate Research: Stratosphere (IEK-7), 52425, Juelich, Germany, m.geldenhuys@fz-juelich.de, markusgeld@gmail.com, +49 163 629 3218

and radiosondes, to answer this question. Turbulent features were successfully characterised by Froude numbers, the Froude-derived height scale and the thermal wind equation. The Bernoulli equation, which classifies gap flow, was not helpful due to the effect of the upwind blocking area. Phenomena in descending order of wind strength produced; compressional effect (44.7 ms^{-1}), blocking (26 ms^{-1}) and lastly, gap flow. Gap flow negatively impacted blocking jet strength. Phenomena in descending order of turbulence intensity; gap flow, mountain wave/rotors and lastly, blocking. Gap flow produced greater vertical velocities than mountain waves. These mountain waves were the most intense vertical velocities measured to date in South Africa, associated with the shortest wavelength waves. Blocking jets of 600m deep, 80 km wide and extending 30km downwind of its exit region was found to modulate mountain wave characteristics significantly. A combination of mountain waves, gap flow and blocking was most likely responsible for the crash, highlighting that these three features cannot be seen as separate processes.

Keywords: Turbulence, Blocking, Gap flow, Mountain wave, Small-scale topography, Coastal mountain

1. Introduction

On 16 December 2015, a Cessna 182Q aircraft crashed in a gap within the Kareedouw-Tsitsikamma Mountains in South Africa (see the “X” in the inset of Fig 1). Two passengers were killed and the pilot was injured (Van der Mescht and Geldenhuys 2018). Analysis of meteorological information revealed that mountain waves were present while blocking and gap flow were likely contributing factors. The Civil Aviation Authority of South Africa incident reports identified many turbulence-related crashes, of which mountain waves were the most prominent cause. Only one crash report mentioned gap flow. No crash reports mentioned blocking, which indicated that these phenomena are rarely hazardous enough to result in a crash or they are not recognised in the South African aviation industry. No gap flow (or blocking) studies were found in South Africa. Internationall, no observational study could be found in a such a small scale environment; highlighting the need for such a study. The aim of this article is to improve aviation forecasts provided by forecasters, by addressing the fine scale interactions of these features from a forecasters perspective during a convergence of events.

Annually, the worldwide aviation industry spends $100 million on turbulence-related injuries. According to the Australian Government (2014), turbulence is normal and frequent. It is a threatening phenomenon and is responsible for the most weather-related in-flight injuries. Turbulence is produced by variances in wind flow. Mountain waves, gap flow and blocking are three turbulence-producing features that can occur when wind flow encounters terrain (Gaberšek and Durran 2004). As subcritical Froude flow (Fr<1) approaches a barrier, the barrier blocks the wind (De Foy et al. 2006; Wallace and Hobbs 2006). Now the wind takes the approach of least resistance around the barrier (gap flow). However, if sufficient momentum is available, the wind overshoots the terrain and creates mountain waves. Downstream hydraulic jumps occur for transitional Froude values (Fr~1) (Barry 1981).

Fig 1 *The topography of the study area and its surroundings. The top left inset indicates the location of the study area (X) relative to South Africa. Points A to D represent the radiosonde release locations, while the permanent AWS network consists of the Gibson Bay wind farm (which is owned by the Council for Scientific and Industrial Research (CSIR)), and the Cape St Francis and Port Elizabeth AWSs (which are owned by the South African Weather Service (SAWS)). The study pass is enlarged in the top right inset with the semi-permanent AWSs numbered 1 to 4.*

Blocking is the obstruction of colder, statically stable upslope flow on the upwind side of a mountain barrier, forming a low-level upwind jet (American Meteorological Society 2012; Overland and Bond 1995). Blocking is characterised by an increase in wind speed, an increase in pressure (as cold air dams against the ridge) and a wind direction shift parallel to the ridge. Pre- and post-frontal synoptic conditions were identified as leading to blocking in

the French Alps (Chen and Smith 1987; Neiman et al. 2010; Overland and Bond 1995), with the jet maintained by a high-pressure ridge after the passage of the front (Neiman et al. 2010). Parameters that describe the characteristics of blocking includes, the Froude number, Froude derived height scale, Rossby radius equation and the thermal wind equation.

Gap winds are classified as a low-level accelerated wind phenomenon. Momentum, thermal forcing or the pressure gradient force accelerates the wind through a gap in the topography (Gaberšek and Durran 2004). Gap flow is frequently observed as cold post-frontal air that is partially blocked by a mountain barrier (American Meteorological Society 2012). The advection of dense, stable and cold air makes the air reluctant to ascend the barrier and it prefers to advance through the gaps (Bradbury 1992a). The smallest gap flow study found in literature had a gap of 5km wide and 600m deep, on St. Vincent Island, Carribean (Smith, et al. 1997). This highlights the importance of this study with a gap width of 1.4km and 280m deep (see section 2.1).

A *mountain wave* is an atmospheric gravity wave that is formed as statically stable air passes over a mountain (Durran 2003). During all mountain wave types, two features are always formed: a single vertical propagating wave over the ridge (Durran 2013) and rotors below the respective waves. Rotors form at ridge height and are a circulation of flow around an axis parallel to the mountain range (American Meteorological Society 2012). Synoptic conditions that lead to mountain waves are variable. Although the International Civil Aviation Organization (2005) states that passing cold fronts can trigger mountain wave development, forecasters still regard post frontal air as unstable and do not consider mountain wave development. Feltz et al. (2008) observed the disintegration of a trapped wave system with the passing of a cold front. South African mountain waves, which produce severe turbulence, are known to occur during pre-frontal northwesterly flow (Van der Mescht and Eloff 2013).

During the T-Rex campaign it was found that mountain wave amplitudes are enhanced by blocking in the Sierra Nevada Mountains (Doyle et al. 2011). However, earlier Smith et al. (2002) found blocking to reduce the mountain wave amplitude at generation. Despite this contradiction, mountain waves coinciding with a blocking regime remains a rarely studied phenomena. Studies of gap flow interacting with mountian waves do exist (e.g. Gaberšek and Durran (2004)), however, none exist for a small scale mountaineous area like in this study.

During *turbulence*, the presence of directional shear, combined with horizontal shear, has a compounding effect on its intensity. There are no rigid rules to determine the severity of turbulence (De Villiers and Van Heerden 2001). Multiple parameters attempt to quantify the severity of turbulence, two of which are the Ellrod Turbulence Index (Eq. 1) and the Richardson number. The Ellrod Turbulence Index highlights turbulence generated by

multiple systems, including mountain waves (Ellrod and Knapp 1992), but does not successfully predict all turbulent cases and their severity (De Villiers and Van Heerden 2001). Pilots have attributed this to the weakness of turbulence indices because they do not consider air density. In dense air, the net air flow over the wing is not the same as in less dense air. Grubišić and Lewis (2004) followed the approach to classify mountain wave intensity with regard to wavelength, amplitude and vertical velocity.

$$\text{Ellrod Turbulence Index} = \left[\left(\frac{\partial u}{\partial x} - \frac{\partial v}{\partial y}\right)^2 + \left(\frac{\partial v}{\partial x} - \frac{\partial u}{\partial y}\right)^2\right]^{\frac{1}{2}} \times \frac{\partial u}{\partial z}; \quad \text{(Eq. 1)}$$

This article discusses the results of an experiment that was conducted to prove blocking, gap flow and mountain wave interaction in a low mountain height and unstable post-frontal regime. These three features interacted over a complex, small-scale coastal mountain range producing turbulence. The remainder of this section provides background information on turbulence-producing phenomena. In Section 2, the basics of the experiment, the instrumentation and the parameters employed are discussed. In Section 3, detail is provided about the data from the semi-permanent automatic weather station (AWS) network around the study site in order to demonstrate the characteristics of blocking. The second part of Section 3 details the findings of one of the field experiments. This is supplemented, where necessary, by results from some of the other field experiments in order to demonstrate specific phenomena. The last two sections provide the discussion and conclusions.

2. Experiment and methods

All heights mentioned in this study are above mean sea level (AMSL) unless otherwise stated and all times are in South African standard time, coordinated universal time (UTC) +2. To simplify the discussion, all winds between 180° and 270° were collectively referred to as southwesterly winds. The experiment consisted of surface observation over an 11-month period, as well as several field experiments where radiosondes were released. Below a description is provided on the study-site, however, more information on the experiment design is discussed in Geldenhuys et al. (2018).

2.1. Study site

The study area is known as the Kareedouw Pass (see Fig 1), which experiences frequent frontal weather. The pass is situated between the Tsitsikamma-Kareedouw ridge, which has an orientation of 290° to 110° and peak heights that vary from 530 m to 819 m (translating to 310 m and 600 m above ground level). Africa Peak, which borders the pass to the west, measures 819 m and has a mountain half-width of 861 m. The pass forms a gap

that is 1.4 km wide and has a low point of 460 m, making the gap 280 m deep. No similar or smaller-scale observational study was found in literature.

The semi-permanent observational network consisted of an AWS on Africa Peak (Point 1 in Fig 1), two AWSs in the gap – St1_baro (Point 2 in Fig 1) and Camo (Point 3 in Fig 1) – and an AWS on the upwind side – Midvalley (Point 4 in Fig 1). The Africa Peak wind sensor sustained wind damage shortly after deployment, providing incorrect wind direction and speed measurements. The wind direction was corrected, but the wind speed was left as measured. It was used as an under-representation. Data from three permanent AWSs were also available (see Fig 1). These AWSs were at Port Elizabeth and Cape St Francis (owned by the SAWS) and at the Gibson Bay wind farm (owned by the CSIR). The Port Elizabeth AWS is located furthest away from the study site and represents environmental conditions uninfluenced by the mountain.

During all six events, 19 radiosonde measurements were conducted using InterMet Africa Systems radiosondes (www.intermetafrica.co.za) and Air Liquide hydrogen gas, aiming for a ±3 ms^{-1} ascent rate. The radiosonde experiment consisted of an upwind radiosonde (see Point A in Fig 1), a radiosonde in the gap (see Point B in Fig 1) and two lee-side radiosondes – at Midvalley (Point C in Fig 1) and Suuranys (Point D in Fig 1). Additional experiments were conducted using party balloons, smoke grenades, tethersondes, parasails, simultaneous ascents, dropsondes and dronesondes. Of which the dronesondes exhibited much promise and warrants further investigation. However, only the results from the AWS and radiosonde data are discussed in this article.

2.2. Methods

All the parameters were calculated using the AWS and radiosonde data. Turbulence was quantified with AWS data by using only wind speeds exceeding 7 ms^{-1} and calculating the standard deviation of the 10-minute average wind speeds ($\sqrt{\frac{\sum(u_{10\min\ avg}-\bar{u})^2}{n-1}}$), as well as the standard deviation of average wind speed from the gusts ($\sqrt{\frac{\sum(u_{gust}-u_{10\min\ avg})^2}{n-1}}$). The wind speed of 7 ms^{-1} is considered to be a sensible threshold, as it disregards variable winds and is the prescribed minimum for mountain wave formation (Barry 1981). Larger values of standard deviation indicate wind variability in addition to greater wind irregularities and are thus a measure of turbulence.

The radiosonde data gathered during the field experiments were used to quantify turbulence by, among other things, the Richardson number, Ellrod Turbulence Index, vorticity, updrafts or downdrafts, and wind direction and speed changes. The potential temperature and cumulative normalised ascent rate were used to visualise turbulence (Feltz

et al. 2008; Grubišić and Billings 2007; Overland and Bond 1995; Van der Mescht 2012). The normalised ascent rate highlights all the updrafts, downdrafts and the disruption of laminar flow (disruption of a smooth graph – see Fig 8 between 2 800 m and 3 200 m). On this graph, a steep slant indicates intense vertical velocities, and a long, steady slant indicates a near-normal ascent rate.

3. Results

3.1. Automatic weather station data analysis

The westerly winds of Gibson Bay wind farm's wind rose (see Fig 2) indicate that blocking occurs on the upwind side of the ridge. The wind roses at Cape St Francis and at the wind farm differ from the environmental wind rose (the Port Elizabeth wind rose) (see Fig 2) and closely simulate one another. The environmental southwesterly winds are deflected and the wind directions at the wind farm and at Cape St Francis are nearly parallel to the Kareedouw ridge. The Cape St Francis station is located approximately 30 km downwind of the Kareedouw ridge. Therefore, the blocking jet extends at least 30 km downwind of its exit region. Africa Peak is located at 819 m AMSL and the wind rose in Fig 2 (see Point 1) shows an anticlockwise shift in wind direction compared to the wind roses at the wind farm and at Cape St Francis, which indicates that, on average, the blocking layer does not extend up to peak height.

Fig 2 *A map of the study site and the surrounding area. Grey represents all topography higher than 500 m AMSL. Wind roses (named as in Fig 1) represent winds when the environmental winds (Port Elizabeth) measured 180º to 270º (southwesterly) with speeds ≥ 7ms^{-1}. The standard deviations are indicated below the wind roses (deviation from average wind speeds or deviation from gust). All wind roses are plotted in a manner similar to the one at Cape St Francis and represent a 70% frequency wind rose, which means that the outer ring represents 70% of the winds. Note the strong deviation of flow in the gap (see points 2 and 3 at the bottom of Fig 2) compared to the permanent stations (top).*

Gap flow is identified on the wind roses (see Fig 2) through wind direction rather than wind speed. Not considering Africa Peak wind speeds, the average wind speeds in descending order of strength are Cape St Francis (blocking regime) 5.8 ms^{-1}, Port Elizabeth (environmental wind) 5.6 ms^{-1} and Camo (gap wind) 5.5 ms^{-1}. Even though the gap wind is relatively weak (see Point 2 in Fig 2), the gap flow is evident in the 60° to 90° wind direction deviation (southerly to southeasterly winds) compared to the blocking region (Gibson Bay wind farm, for instance). However, the along-barrier wind direction of the blocking jet greatly reduces the cross-sectional area and the exposure of the gap, which limits the gap flow intensity. Rather than winds funnelling through the gap (as in conventional Venturi or

Bernoulli theory), blocking drives gap flow by air spilling through the gap or by enhancing the temperature and pressure gradients across the ridge.

The strongest 10-minute average wind was measured at Africa Peak (see Point 1 in Fig 2) with a wind speed of 35.2 ms^{-1} and a gust of 44.7 ms^{-1}. These strong winds are attributed to the acceleration of the compressional effect above the ridge (similar to that suggested by Barry (1981)). Camo AWS (see Point 3 in Fig 2) measured the second-highest 10-minute average wind speed of 23.2 ms^{-1} and a gust of 32 ms^{-1}. The relatively low standard deviation values for the average 10-minute wind speed at this station indicate little variability, which means that the wind speeds are more consistent. In contrast, the high standard deviation for the wind gust at Camo AWS shows that this location experiences larger differences between the 10-minute average wind speeds and wind gusts. This infers stronger gusts or gusts that occur more frequently at the Camo AWS, second only to Port Elizabeth.

3.2. Event analysis

The event of 26 October 2017 is used here as it exhibited a full experimental dataset. Blocking, gap flow and mountain waves were evident on this day. Furthermore, this was the only event where satellite altimetry was available and allowed for a thorough investigation of the wind profiles. There was no precipitation during this event and it is therefore classified as not being influenced by precipitation-induced downdrafts. The remnant of the weakened tail of a cold front is observed with cold air cumulus behind it on the bottom right of the satellite image (valid for 26 October 2017, see – Fig 3).

Fig 3 *A high-resolution, visible satellite image at 14:00 on 26 October 2017 highlighting a stationary wave (block) and the study gap (arrow). Copyright EUMETSAT 2018.*

On this day, a cold front (supported by a broad mid-level trough up to 500 hPa) passed south of the study site, followed directly by a ridging surface high pressure system. Satellite altimetry confirms southwesterly winds over the ocean deflected to along-shore or along-barrier winds (in the oval area in the left inset in Fig 4), with the wind speeds broadly increasing towards the coast. Unfortunately, the satellite did not pass directly over the study site, but general wind direction tendencies infer along-barrier wind directions south of the study site (indicated by the long arrow in Fig 4b). The change in wind direction near the coast was consistent with a pressure nose (ridge) on the mean sea level pressure map (not shown). The pressure nose formed as the pressure increased upwind of the barrier in the blocking area, altering synoptic conditions (as in Overland and Bond (1995)).

Fig 4 *A map of the area surrounding the study area depicting surface and radiosonde winds on 26 October 2017. Winds at the Gibson Bay wind farm, Cape St Francis, as well as station 1, 2 and 3 (named as in Fig 1) are surface winds. At this time, the Africa Peak wind sensor was confirmed to be faulty and it is most likely an under-representation of wind speeds. The lines emanating from points A to D demarcate radiosonde flight paths on this day (named as in Fig 1) with wind barbs indicating the wind at ridge height (819 m). All flight paths have a dominant west-to-east direction, but with deviations in the gap (see Point B in Fig 4c) and in the wave over the Suuranys ridge (indicated by X in Fig 4a). The bottom left inset (Fig 4b) is a satellite altimetry image from NOAA ASCAT-B at 08:46, indicating the position of the cold front and the change in wind direction in the oval. The bottom right inset (Fig 4c) is an enlargement of the study gap (Point B) and illustrates the winds from the surface AWS network. A triangle flag on a barb indicates 25 ms^{-1}, a single flag indicates 5 ms^{-1} and a short or half flag demarcates 2.5 ms^{-1}. Shaded grey areas represent topography higher than 500 m AMSL.*

3.2.1. Blocking

A blocking jet was present during all field experiments with a maximum upwind wind speed between the gap and ridge height (460 m to 819 m). Generally, the cross-barrier wind speed (v̀) increased from the surface to well above the mountaintop. The upwind radiosonde represents the data of the blocking jet of 26 October 2017 (see Point A in Fig 1). The layered Froude number (see Fig 5) was calculated to be a minimum (~0.14) from 260 m to 460 m, specifying the area of maximum blocking. A sharp increase in the Froude number (see Fig 5) and the ù wind (see the red bold solid lines in Fig 6b), suddenly tapering off from 460 m to 700 m, implies a weakening in the blocking regime. This occurs at gap height as air spills through the gap. The Froude derived height scale ($h_1=\frac{\bar{v}}{N}$, when Fr is set to 1; where $\bar{v}$ is the averaged wind speed, from surface to peak, of the cross-barrier component of the wind perpendicular to the mountain (Van der Mescht and Eloff 2013) and $N=\sqrt{(g/\bar{\theta})(\frac{\partial\theta}{\partial z})}$ is the Brunt-Väisälä frequency) accurately suggested a shallow blocking jet with a top of 420 m to 510 m AMSL; confirming gap flow weakens the blocking jet by 'spilling' ($h_{gap}<h_1$ (Overland and Bond 1995)). Provided the Froude number was less than 1 (see Fig 5 below the mountain peak), the Rossby radius equation ($L_R=\left(\frac{Nh_m}{f}\right)F_m=\frac{\dot{v}}{f}$, when $F_m<1$; where h_m is the mountain height from surface to mountaintop and f is the Coriolis parameter (Overland and Bond 1995)) suggested a jet width of 39 km, and the thermal wind equation ($\Delta V=\frac{N^2h^2}{fL}=$v̀, when $F_m<1$; where is the mountain half-width (Overland and Bond 1995)) proposed a 3.1 ms^{-1} increase in the along-barrier wind speed (ù). Satellite altimetry observations (see Fig 4b) indicate that this blocking region exists and illustrates an increase in wind speed consistent with the thermal wind equation (Overland and Bond 1995). Satellite altimetry proposes a jet width of at least 80 km contrasting the Rossby radius equation suggestion of 39 km by the wind direction change to a barrier parallel wind direction.

Fig 5 *The calculated layered Froude parameter (layered from the surface to the respective height) from the upwind radiosonde released at 06:30 on 26 October 2017. The dash-dot line indicates the height of Africa Peak and the dashed line is the height where the radiosonde passed over the ridge (3 350 m).*

During the field experiments, the strongest blocking jet occurred on 8 June 2017. The wind speed measured 26 ms^{-1} (see the blue dots in Fig 6 and 7) with a 24 ms^{-1} ù (along-barrier) and 9 ms^{-1} ѵ (cross-barrier) wind. The maximum wind speed (26 ms^{-1}) occurred at mountain height (see Fig 6a), which increases by 11 ms^{-1} from the surface (15 ms^{-1}). The change in wind direction (see Fig 7b above 800 m) and decrease in along-barrier wind speed (ù – see the blue dotted line in Fig 6b above 810 m) above mountain height indicate a rapid deterioration in blocking characteristics.

The blocking area was a turbulence-free zone, which is illustrated by little to no fluctuations in the Ellrod Turbulence Index (see Fig 7c). The uniform increase with height of the wind direction and speed of the blocking jet resulted in little turbulence on 8 June 2017 and 26 October 2017 (see Fig 7a to 7c). During the field experiments, turbulent areas occurred directly above the blocking jet and the ridge height (800 m to 1 300 m). This transition zone experiences large wind direction and speed changes, where the deflected blocking jet returns to environmental flow and interacts with winds feeling the barrier and the frequently contrasting environmental background wind flow.

Fig 6 *Along- (ù) and across-barrier (ѵ) winds of all upwind radiosondes. All events had a mountain Froude value of less than one (not indicated), indicating blocking conditions.*

3.2.2. Gap flow

In all events, both AWS and radiosonde data indicated that the gap wind speed was significantly lower than the blocking jet. This demonstrates that, when evaluated for wind strength only, the blocking region produces a stronger jet than the gap region. On 26 October 2017, the weakening in the blocking region, at gap height (see Fig 5) proves that gap flow is present. Gap divergence or an eddy emerges in the radiosonde flight paths (see the right inset in Fig 4) with rapid wind direction changes between the surface and 700 m from a southerly to a westerly direction. A diverging wavelike flight path with changing Froude values, rapid discontinuities in wind speeds and a potential temperature inferred plot suggested an expansion fan, as in Colle and Mass (1998) and Saito (1992). However, this will be subject to further investigation in a future study.

Fig 7 *The wind speed and direction for the two blocking cases of 8 June and 26 October 2017. The Ellrod Turbulence Index for 8 June indicates virtually no turbulence in the blocking region.*

Other indications of turbulence on 26 October 2017 included peak clockwise rotational values at 480 m, 540 m and 630 m (listed according to the descending strength of vorticity values and calculated perpendicular to the ridge). The peak clockwise rotational values coincided with constant potential temperatures and subcritical Richardson values (values below 0.25 (Doyle et al. 2009)), which all suggest severe rotors (classified according to Hertenstein and Kuettner (2005) and Van der Mescht and Eloff (2013)) or a hydraulic jump. The first anticlockwise rotational peak observation was shortly above the mountaintop. This was identified as a rotor and is expectantly mountain wave or thermal related. Thermals generated by the warm northerly slope interact with colder air and spill over the mountain, which can produce rotors (or cavity rotations, as in Wallace and Hobbs (2006)). It is worth mentioning that, on 13 December 2017, a smoke grenade attached to the gap radiosonde revealed a rotor rotating along a north-to-south axis below the mountaintop at approximately 700 m AMSL. Vorticity values along a north-to-south axis confirmed this unexplained rotation during multiple events. All but one case portrayed rotational areas as peak turbulence values on the Ellrod Turbulence Index.

The maximum updraft and downdraft in the gap region in this study included 6.6 ms^{-1} (on 26 October 2017) and 6.8 ms^{-1} (at 517 m on 8 June 2017). The peak downdraft on 8 June 2017 was followed by the ascent's peak updraft of 4.5 ms^{-1} at 527 m. This downdraft recorded in the gap region exceeded the downdrafts recorded above mountain height (2.1 ms^{-1}), that is induced by mountain waves. Even though there was only a modest mountain wave event on 8 June 2017, it is evident that gap flow can occasionally produce more severe vertical velocities than mountain waves. The sharpest increase in wind speed, with a change from 4.3 ms^{-1} at the surface to 18.8 ms^{-1} at peak height, was also measured on 8 June 2017.

Wind profiles of all gap ascents indicated a sheared environment in wind direction and speed. All (but two) gap radiosondes indicated wind speeds that increased rapidly up to ridge height, whereby the wind speeds weakened or remained constant in height. Such turbulent variations in winds, updrafts and downdrafts, combined with rotors, were observed by multiple gap radiosondes.

3.2.3. Mountain waves

On 26 October 2017, an evolution of mountain waves was observed (see Fig 3). The Midvalley radiosonde (see Point C in Fig 4) penetrated this mountain wave system and experienced a deflection of flow in the wave. This unexplained phenomenon, which was observed during more than one ascent, is the cross-barrier wind speed (v̀) that mimics the

cumulative normalised ascent rate (see Fig 8). A decrease in the cross-barrier wind speed (v̀) correlates with the downdraft (leftward slant) and vice versa. The Ellrod Turbulence Index highlighted the peak downdraft area and the disruption of laminar flow (see Fig 8) as turbulent, contrary to the updraft area. The Ellrod Turbulence Index indicated all identified rotors as turbulent, except one mid-valley rotor at 1 500 m. One severe rotor was classified by the potential temperature remaining constant from the surface up to 1 600 m, a chaotic vorticity region (indicating multiple clockwise and anticlockwise rotations) and Richardson values below 0.25.

The definition of Grubišić and Lewis (2004) of the parameters measured on 26 October 2017 reveals moderate mountain waves. An 8 km to 10 km wavelength (determined from satellite imagery), and a peak updraft (8.3 ms^{-1}; at 1 450 m) and downdraft (3.3 ms^{-1} at 3 950 m) were determined. The classifying criteria of most events revealed a dominant moderate mountain wave and, at times, a mixture of criteria in the severe category.

Fig 8 *(a): The cumulative normalised ascent rate; (b): the Ellrod Turbulence Index; and (c): the ù (dotted) and v̀ (dashed) winds of the Midvalley radiosonde on 26 October 2017. Note the disruption of laminar flow (smooth graph) between 2 800 m and 3 200 m in Fig 8a.*

On two mountain wave occasions (31 August 2017 and 13 December 2017), downdrafts caused radiosondes to lose height for prolonged periods. On 13 December 2017, a loop sounding (see Fig 9) was observed by the gap radiosonde that penetrated the visible mountain wave in Fig 9a. The gap radiosonde measured a maximum updraft of 6.7 ms^{-1} (below ridge height) and 5.6 ms^{-1} (at 3 400 m) with a peak downdraft of 5.1 ms^{-1} (3 800 m losing 200 m altitude over 6.1 km). The duplication of data at 4 000 m on the skew-T represents the radiosonde losing altitude. Note the signature of lifted mixing layers between 1 000 m and 2 500 m, as well as 2 500 m to 3 800 m. It is evidence of the mixing produced by the mountain waves. Likewise, note how the temperature mimics the dry-adiabatic lapse rate in the downdraft and the moist adiabatic lapse rate at the top of the updraft.

Observations of mountain waves were evident in radiosonde data and/or satellite imagery in five of the six events. The mountain waves in this study originated from small-scale topography, yet it observed updrafts, downdrafts and rotors similar to other studies in larger topographical areas. This study observed mountain wave-related vertical velocities of up to 8.3 ms^{-1}. In comparison, Feltz et al. (2008) observed vertical velocities of 4 ms^{-1} in the Rockies. Van der Mescht and Eloff (2013) observed 7.2 ms^{-1} in the Hexriver Mountains, and

Grubišić and Billings (2007) observed 10 ms^{-1} in the Sierra Nevada Mountains, which has an average climb of 3 000 m over 10 km.

Fig 9 *The gap radiosonde skew-T photographs of mountain wave features and the wind measured on 13 December 2017. Left: On the skew-T, the solid red and blue lines represent the temperature and dew point temperature respectively. The dashed line demarcates the cumulative normalised ascent rate, indicating the updrafts (rightward slant) and downdrafts (leftward slant) of the ascent. Middle: Photographs of visible wave features observed on 13 December 2017. The main photograph of the lenticular cloud (a); and the Kelvin-Helmholtz waves (d) – observed on top of an adjacent lenticular cloud – was taken upwind of the barrier, while the rotor clouds (dashed outline in (b) and (c) were observed in the lee. The Kelvin-Helmholtz waves probably formed because of the streamlines converging on top of the mountain wave, resulting in instability in the system, as the more rapid wind speeds on top of the mountain wave and slower wind speeds in the mountain wave interact. Right: The winds (total wind, cross-barrier (ѵ) and along-barrier wind speeds (ù)) demarcating the loop sounding formed by the radiosonde losing altitude.*

4. Discussion

Designing an experiment to observe small-scale complex features such as turbulence and identifying individual phenomena such as blocking, gap flow and mountain waves is complicated at best. The experiments discussed in this paper nevertheless set out to observe small-scale complex features and were able to identify the phenomena to a large extent. It was found that the blocking region positively and negatively influences the formation of both gap flow and mountain waves, with gap flow impacting negatively on blocking. The sea-level pressure increase within the blocking region enhances the pressure gradient across the gap and drives gap flow.

On the other hand, the deflected blocking jet impacts negatively on gap flow by reducing the gap cross-sectional area that is exposed to the wind, resulting in weaker gap wind speeds than the blocking and environmental wind speed. The air flow through the gap reduces the upwind pressure and, in turn, weakens the blocking region. However, blocking is the feature that exacts the most significant influence on the surroundings. The blocking jet peak occurs between gap height and peak height. This is in contrast to the findings of Neiman et al. (2010), who observed the peak at one third of the mountain height.

A lack of satellite altimetry data made the evaluation of the blocking parameters' thermal wind equation and the Rossby radius equation difficult. The Froude-derived height scale and the Froude number compared well with radiosonde along-barrier winds (ù). Contrary to other studies, the Bernoulli equations (for compressible and incompressible fluids as applied in Gaberšek and Durran (2004)) that characterise gap flow did not prove to be helpful during blocking. The temperature being lower in the blocking area than in the gap exit, and air spilling, rather than funnelling into the gap, is deemed to be responsible for the failure of the Bernoulli equation.

Multiple features were observed at the gap exit. A feature simulating an expansion fan was observed in the gap and should be investigated further. Rotating eddies were observed at the gap exit. In this study, the gap jet did not seem to be influenced by mountain waves, contrary to what other studies suggest (Gaberšek and Durran 2004). Similarly, mountain waves were not influenced by gap flow, but rather by the blocking regime via a dynamic barrier, as also described by Neiman et al. (2010).

The experimental results indicated that air approaching the coast is forced to rise above the colder dynamic barrier, which is walled by the mountain. At ridge height, the along-barrier blocked flow and the air above the dynamic barrier accelerate down the lee slope into the transitional flow, forming a mountain wave. This process is well documented and also explained by Barry (1981) and Feltz et al. (2008).

In this study, blocking was found to be the least turbulent area and the gap was found to be the most turbulent regime. The blocking region had the strongest winds. However, the uniform changes in wind direction and speed (see Fig 4 and 6) produced the least turbulence. Large changes in wind direction and speed are observed directly above the blocking region, indicating turbulence. Wind speeds in the gap were generally weaker than in the blocking regime. However, significant turbulence was identified here, given that directional shear is described to have a compounding effect on wind speed shear (Ellrod and Knapp 1992). In one experiment (8 June 2017), the gap winds increased in strength by 15 ms^{-1} over 250 m with a 55° wind direction change over 100 m. The large variety of features observed in the gap and their contrasting nature makes this a meteorologically complex area and should best be avoided by pilots.

Occasionally, gap-flow-induced updrafts and downdrafts exceeded those caused by mountain waves, thereby creating a hazard more dangerous than mountain waves. Mountain waves with severe rotors cause hazardous conditions. Mountain-wave-induced rotors and downdrafts can penetrate down to gap level, causing additional turbulence in the gap. This is another reason why pilots should avoid this area.

The Ellrod Turbulence Index performed reasonably well in identifying turbulent areas. The Richardson number, as a standalone parameter, was less practical and produced much noise when applied to the fine vertical resolution of the radiosonde data. It found turbulent areas throughout the atmosphere. It remains difficult to forecast the severity of mountain wave turbulence, and a nomogram is recommended to aid with this (International Civil Aviation Organization 2005). The study's results indicate that mountain waves with short wavelengths produced greater vertical velocities than those in other studies (Feltz et al. 2008; Van der Mescht and Eloff 2013; Grubišić and Billings 2007) where the wavelengths were longer. It remains an open question, but one has to consider that blocking positively

contributed to greater vertical velocities as was suggested by Doyle et al. (2011). Classifying the severity of mountain waves with regard to wavelength and amplitude was found not to be useful in this study. It is concluded that forecasters and pilots should regards all mountain waves as severe, especially for low-level flying in the vicinity of topography. To the knowledge of the authors, the mountain waves measured in the experiments that formed part of this paper were the most severe mountain waves measured to date in South Africa.

5. Conclusions

On 16 December 2015, an aircraft crashed in a gap within the Kareedouw-Tsitsikamma Mountains, killing two passengers and injuring the pilot. There was a sudden onset of turbulence, which resulted in the pilot losing consciousness 2 km upwind of the crash site (the gap). One of the passengers most likely took control of the aircraft, but crashed directly upwind of the gap exit. The results from the experiments conducted as part of this paper show that the sudden onset of turbulence was likely because of a mountain wave or its associated rotor. It was also shown how the gap is a significant turbulent area. This turbulence, together with blocking, was likely the final contributor to the crash. Aircraft should rather avoid this area.

Interactions between blocking, gap flow and mountain waves are complex. Blocking drives gap flow, where, in turn, gap flow weakens the blocking regime. Blocking also contributed to mountain wave formation by altering incident conditions caused by the dynamic barrier. This feature should be investigated in more detail, especially the possible effect of this on mountain wave intensity.

This study highlights the hazard that small-scale mountain waves pose to aviation and emphasises the lack of knowledge on this feature in the vicinity of small-scale topography, blocking and gap flow. These small-scale mountain waves produced the strongest vertical velocities ever measured in a South African study.

Forecasters, pilots and scientists performing experimental designs should keep the following in mind within mountainous regions;

- Gapflow can provide greater vertical velocities than mountain waves
- Mountain waves, in post-frontal airmasses, are more severe than pre-frontal airmasses
- Mountain wave severity should not be classified according to their corresponding mountain, the stability and wind profiles. It’s a far more complex system.
- Simplistic forecasting of mountain waves and their intensity is not possible.
- Blocking can extend far downwind of its formation area.
- Blocking can possibly assist in inducing greater mountain wave vertical velocities.
- Fly well above the highest point in the vicinity to avoid the compounding effect of different turbulent mechanisms.

- Although winds are weak in the gap, this is the most turbulent area
- Phenomena rated in descending order of wind strength; compressional effect, blocking and lastly, gap flow.
- Phenomena rated in descending order of turbulence intensity; gap, mountain wave/rotor and lastly, blocking.
- Parameters successful for studying this interaction are Froude number, Froude-derived height scale, Ellrod Turbulence Index, vorticity equation, potential temperature plots and the cumulative normalised ascent rates.
- Parameters unsuccessful in characterising flow are Bernoulli equation and the Richardson number; as a standalone parameter.

In conclusion, one cannot look at wind flow in complex terrain simplistically. The three features, blocking, gap flow and mountain waves, are intertwined and cannot be seen as separate processes.

References

American Meteorological Society (2012) Glossary of meteorology, 2nd ed. http://amsglossary.allenpress.com/glossary. Accessed 22 February 2016

Australian Government (2014) Staying safe against in-flight turbulence, 2nd ed. Australian Transport Safety Bureau, pp 1–3

Barry R (1981) Mountain weather and climate. London: Methuen.

Bradbury T (1992a) Sailplanes and gliding. Skywatch – a beginners guide to clouds, August-September, pp 210–215

Bradbury T (1992b) Sailplane and gliding. Skywatch – a beginners guide to clouds, October-November, pp 256–260

Caccia J, Benech B, Klaus V (1997) Space-time description of nonstationary trapped lee waves using ST radars, aircraft, and constant volume balloons during the PYREX experiment. Journal of the Atmospheric Sciences 54(14): 1821–1833. https://doi.org/10.1175/1520-0469(1997)054<1821:STDONT>2.0.CO;2.

Chen W, Smith R (1987) Blocking and deflection of airflow by the Alps. Monthly Weather Review 115(November): 2578–2597.
https://doi.org/10.1175/1520-0493(1987)115<2578:BADOAB>2.0.CO;2.

Colle BA, Mass CF (1998) Windstorms along the western side of the Washington Cascade Mountains. Part I: A high resolution observational and modeling study of the 12 February 1995 event. Monthly Weather Review 126: 28–52. https://doi.org/10.1175/1520-0493(1998)126<0028:WATWSO>2.0.CO;2.

De Foy B, Clappier A, Molina L, Molina M (2006) Distinct wind convergence patterns in the Mexico City basin due to the interaction of the gap winds with the synoptic flow. Atmospheric Chemistry and Physics 6: 1249–1265. https://doi.org/10.5194/acp-6-1249-2006.

De Villiers M, Van Heerden J (2001) Clear air turbulence over South Africa. Meteorological Applications 8:119–126. https://doi.org/10.1017/S1350482701001104.

Doyle JD, Grubišić V, Brown WOJ et al (2009) Observations and numerical simulations of subrotor vortices during T-REX. Journal of the Atmospheric Sciences 66: 1229–1249. https://doi.org/10.1175/2008JAS2933.1.

Doyle J, Qingfang J, Smith R et al (2011) Three-Dimensional Characteristics of Stratospheric Mountain Waves during T-REX. Monthly Weather Review, Volume 139, pp. 3-23. https://doi.org/10.1175/2010MWR3466.1

Durran D (2013) Lee waves and mountain waves. University of Washington. https://www.atmos.washington.edu/2010Q1/536/2003AP_lee_waves.pdf.

Ellrod G, Knapp D (1992) Forecasting techniques – an objective clear-air turbulence forecasting technique: Verification and operational use. Weather and Forecasting 7: 150–165. https://doi.org/10.1175/1520-0434(1992)007<0150:AOCATF>2.0.CO;2.

Feltz WF, Bedka JA, Otkin JA et al (2008) Understanding satellite-observed mountain-wave signatures using high-resolution numerical model data. Weather and Forecasting 24: 76–86. https://doi.org/10.1175/2008WAF2222127.1.

Gaberšek S, Durran D (2004) Gap flows through idealized topography. Part I: Forcing by large-scale winds in the non-rotating limit. Journal of the Atmospheric Sciences, 61: 2846–2862. https://doi.org/10.1175/JAS-3340.1.

Geldenhuys M, Van der Mescht D, Dyson LL, (2018) Poor-man's experimental design: Measuring wind and turbulence in a complex environment. Preprints of the 34th annual conference of the South African Society for Atmospheric Science : 36–39.

Grubišić V, Billings B (2007) The intense lee-wave rotor event of sierra rotors IOP 8. Journal of Atmospheric Sciences 64: 4178–4201 https://doi.org/10.1175/2006JAS2008.1.

Grubišić V, Lewis J (2004) Sierra wave project revisited: 50 years later. Bulletin of the American Meteorological Association 85:1127–1142.https://doi.org/10.1175/BAMS-85-8-1127.

Hertenstein R, Kuettner J (2005) Rotor types associated with steep lee topography: Influence of the wind profile. Tellus 57A: 117–135.
https://doi.org/10.3402/tellusa.v57i2.14625.

Hurd W (1929) Northers of the Gulf of Tehuantepec. Monthly Weather Review 57: 192–194. https://doi.org/10.1175/1520-0493(1929)57<192:NOTGOT>2.0.CO;2.

International Civil Aviation Organization (2005) Manual on low-level wind shear, pp. 137

Neiman P, Sukovich E, Ralph F, Hughes M (2010) A seven-year wind profiler-based climatology of the windward barrier jet along California's orthern Sierra Nevada. Monthly Weather Review 138: 1206–1232. https://doi.org/10.1175/2009MWR3170.1

Overland J, Bond N (1995) Observations and scale analysis of coastal wind jets. Monthly Weather Review 123: 2934–2941.
https://doi.org/10.1175/1520-0493(1995)123<2934:OASAOC>2.0.CO;2.
Pan F, Smith R (1999) Gap winds and wakes: SAR observations and numerical simulations. Journal of the Atmospheric Sciences 56(7): 905–922.
https://doi.org/10.1175/1520-0469(1999)056<0905:GWAWSO>2.0.CO;2.
Saito K (1992) Shallow water flow having a lee hydraulic jump over a mountain range in a channel of variable width. Journal of the Meteorological Society of Japan 70(3): 775–782. https://doi.org/10.2151/jmsj1965.70.3_775.
Smith, R. et al., 2002. Mountain Waves over Mont Blanc: Influence of a Stagnant Boundary Layer. Journal of the Atmospheric Sciences, Volume 59, pp. 2073-2092.
https://doi.org/10.1175/1520-0469(2002)059<2073:MWOMBI>2.0.CO;2
Van der Mescht D (2012) Mountain wave turbulence in the lee of the Hex River Mountains, Stellenbosch: Masters Disertation, Stellenbosch University, Department of Geography and Environmental Studies. http://hdl.handle.net/10019.1/20240.
Van der Mescht D, Eloff P (2013) Mountain wave-induced rotors in the lee of the Hex River Mountains. South African Geographical Journal 95(1): 117–131.
https://doi.org/10.1080/03736245.2013.808077.
Van der Mescht D, Geldenhuys M (2018) Observations of mountain waves with interference generated by coastal mountains in South Africa, Meteorological Applications.
https://doi.org/10.1002/met.1771.
Wallace J, Hobbs P (2006) Atmospheric science: An introductory survey, 2nd ed. Elsevier.

Figure 1

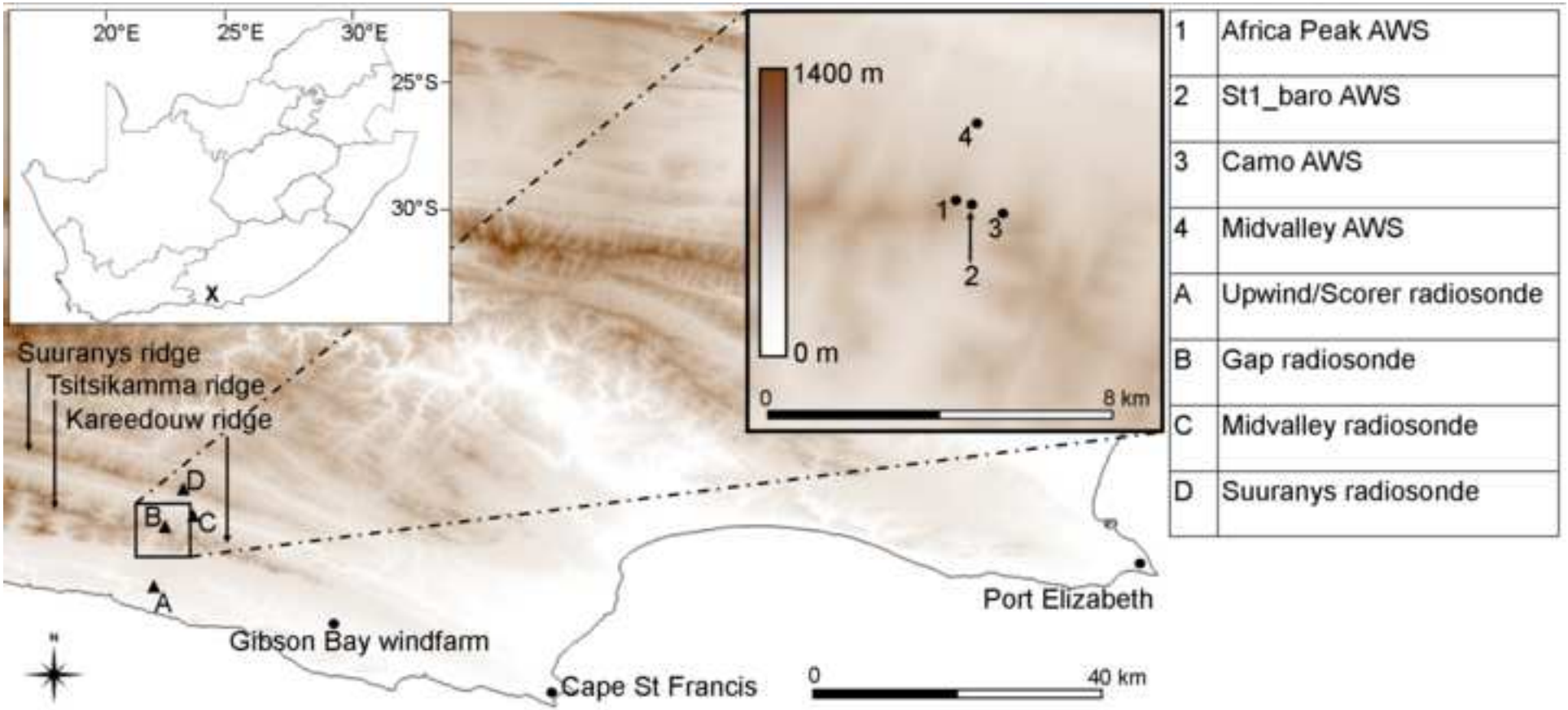
20°E
25°E
30°E
25°S
30°S
X
1400 m
0 m
0
8 km
4
1
3
2
Suuranys ridge
Tsitsikamma ridge
Kareedouw ridge
D
B
C
A
Port Elizabeth
Gibson Bay windfarm
Cape St Francis
0
40 km
1 Africa Peak AWS
2 St1_baro AWS
3 Camo AWS
4 Midvalley AWS
A Upwind/Scorer radiosonde
B Gap radiosonde
C Midvalley radiosonde
D Suuranys radiosonde

Figure 2

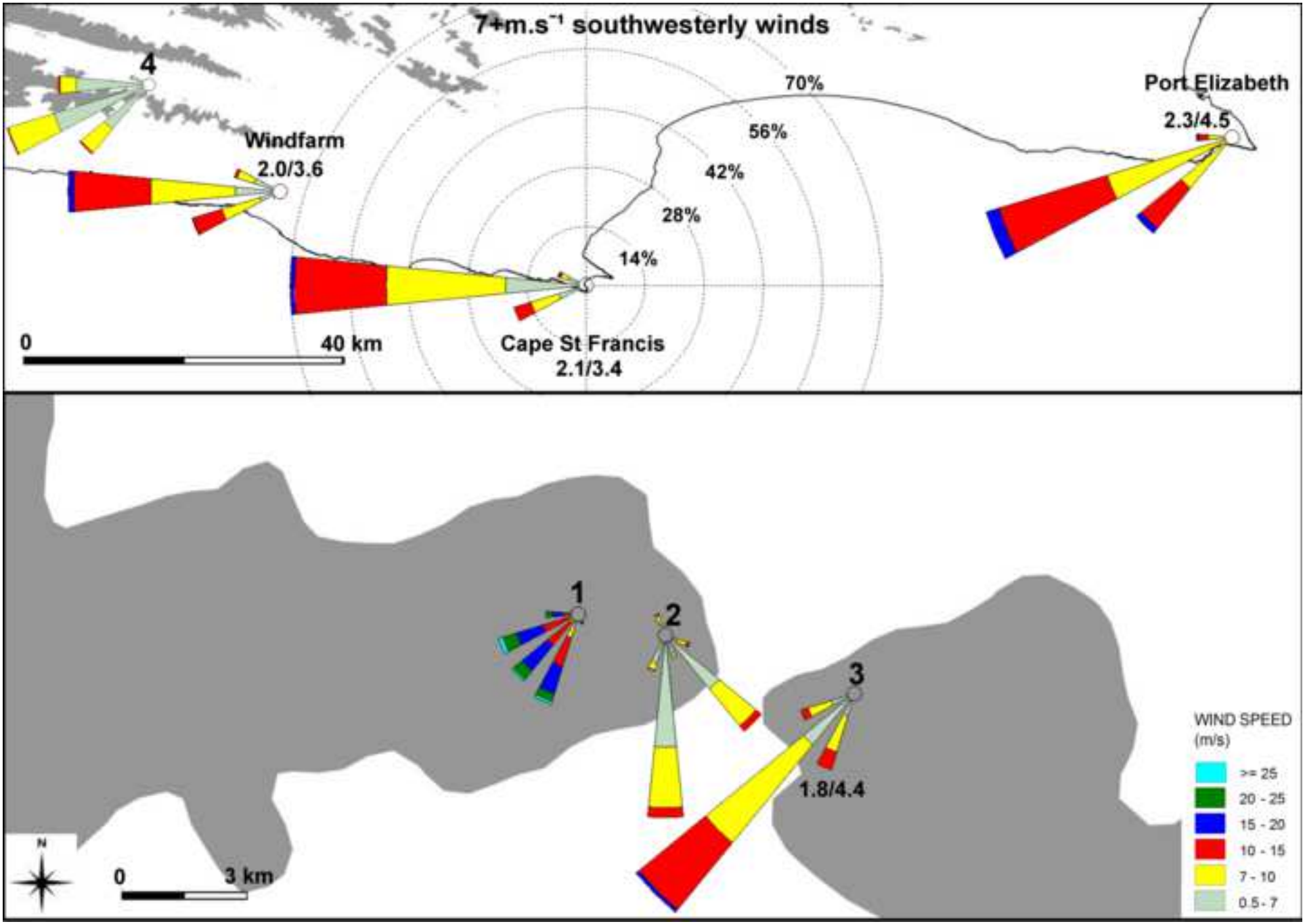
7+m.s⁻¹ southwesterly winds
4
Windfarm
2.0/3.6
70%
56%
42%
28%
14%
Port Elizabeth
2.3/4.5
0
40 km
Cape St Francis
2.1/3.4
1
2
3
1.8/4.4
N
0
3 km
WIND SPEED
(m/s)
>= 25
20 - 25
15 - 20
10 - 15
7 - 10
0.5 - 7

Figure 3

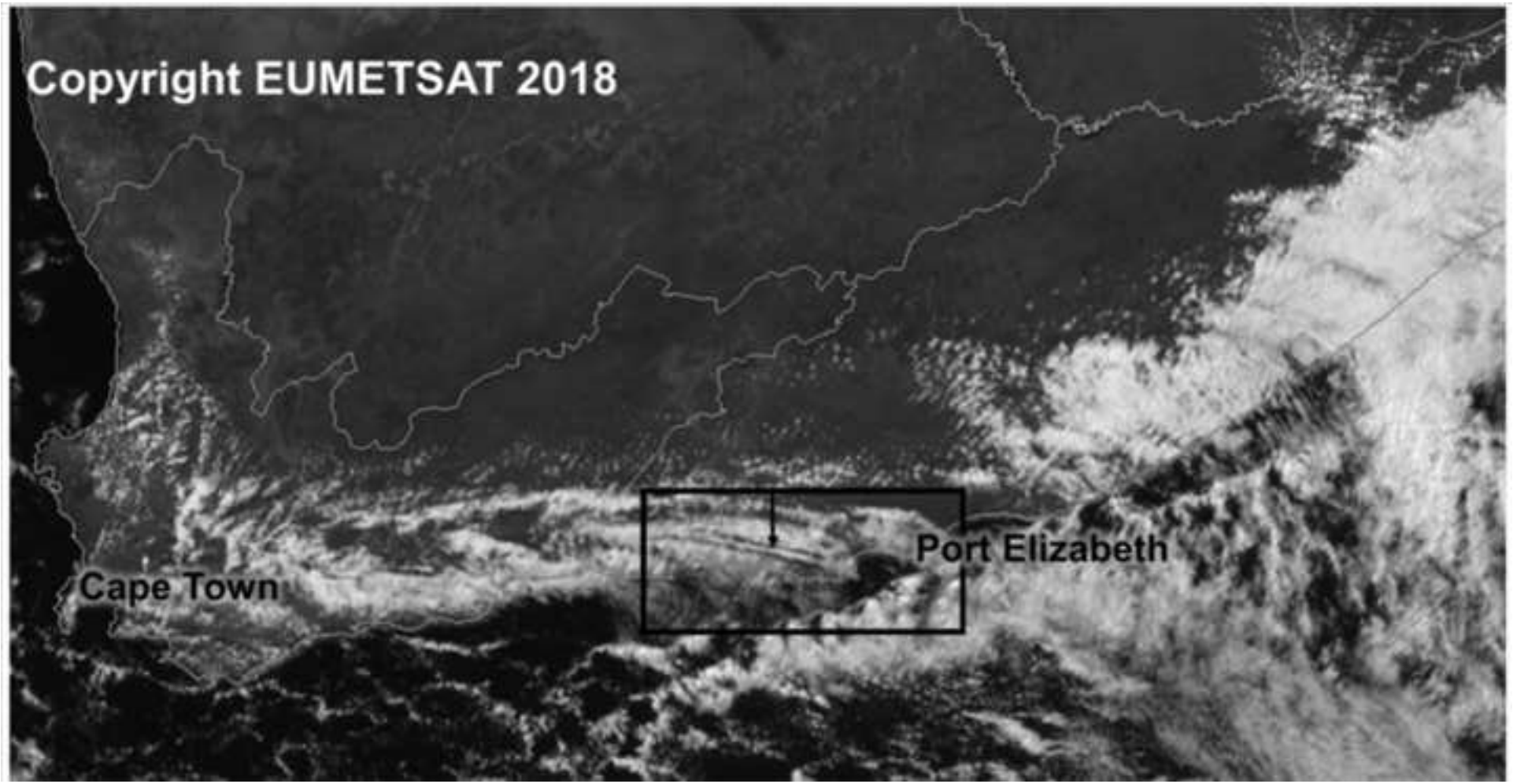

Figure 4

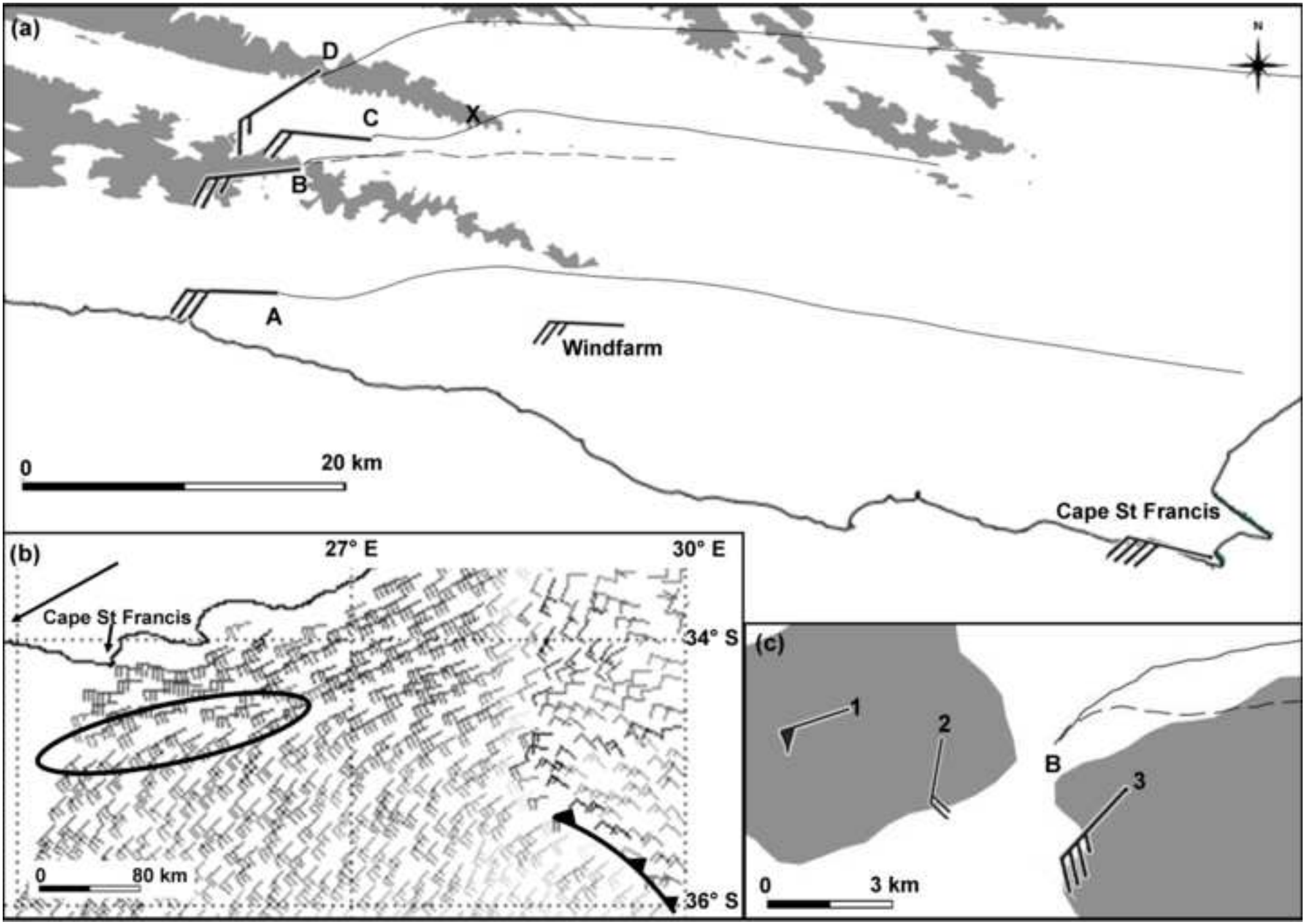
(a)
N
D
C
X
B
A
Windfarm
0
20 km
Cape St Francis
(b)
27° E
30° E
Cape St Francis
34° S
0
80 km
36° S
(c)
1
2
B
3
0
3 km

Figure 5

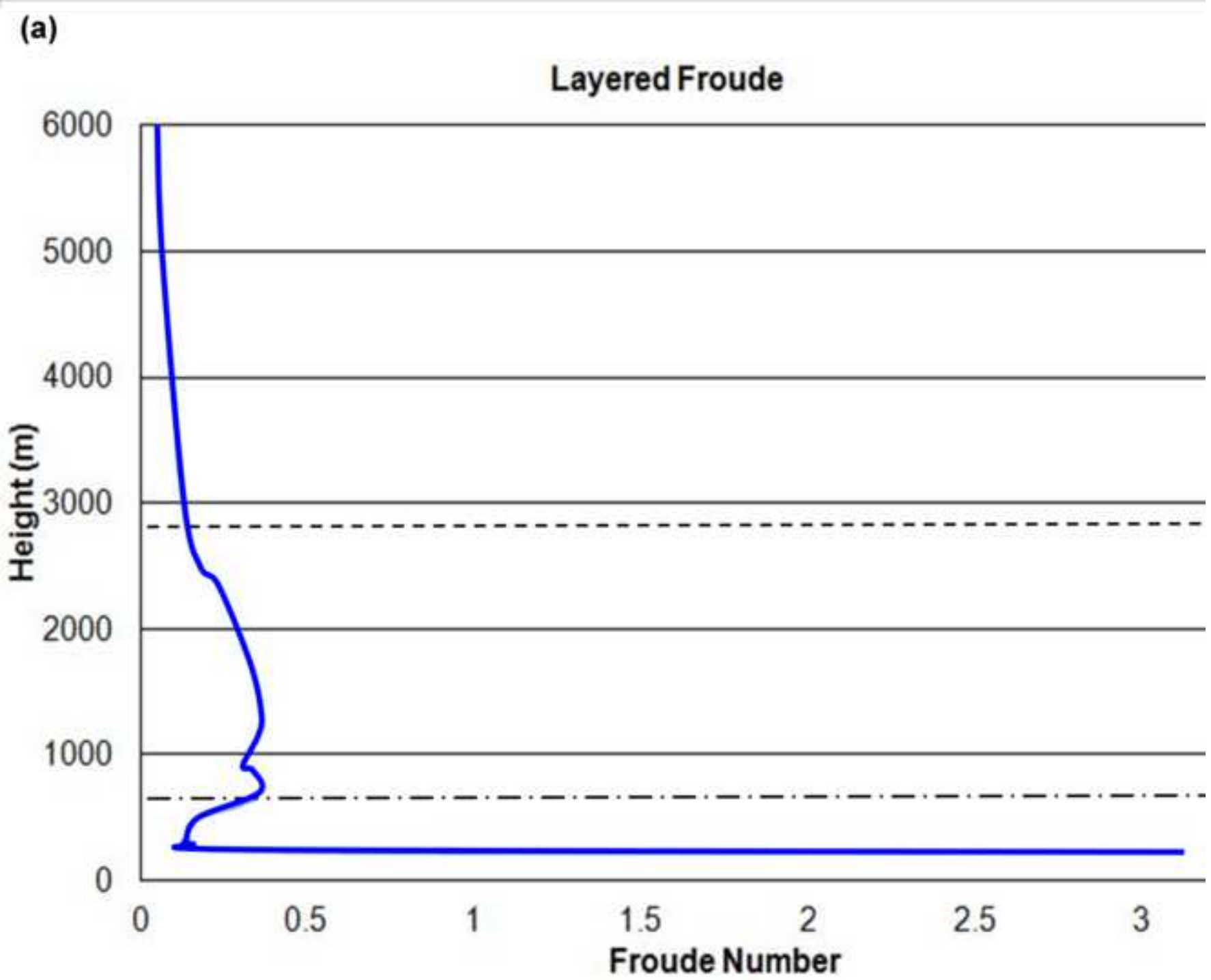
(a)
Layered Froude
6000
5000
4000
3000
2000
1000
0
Height (m)
0
0.5
1
1.5
2
2.5
3
Froude Number

Figure 6

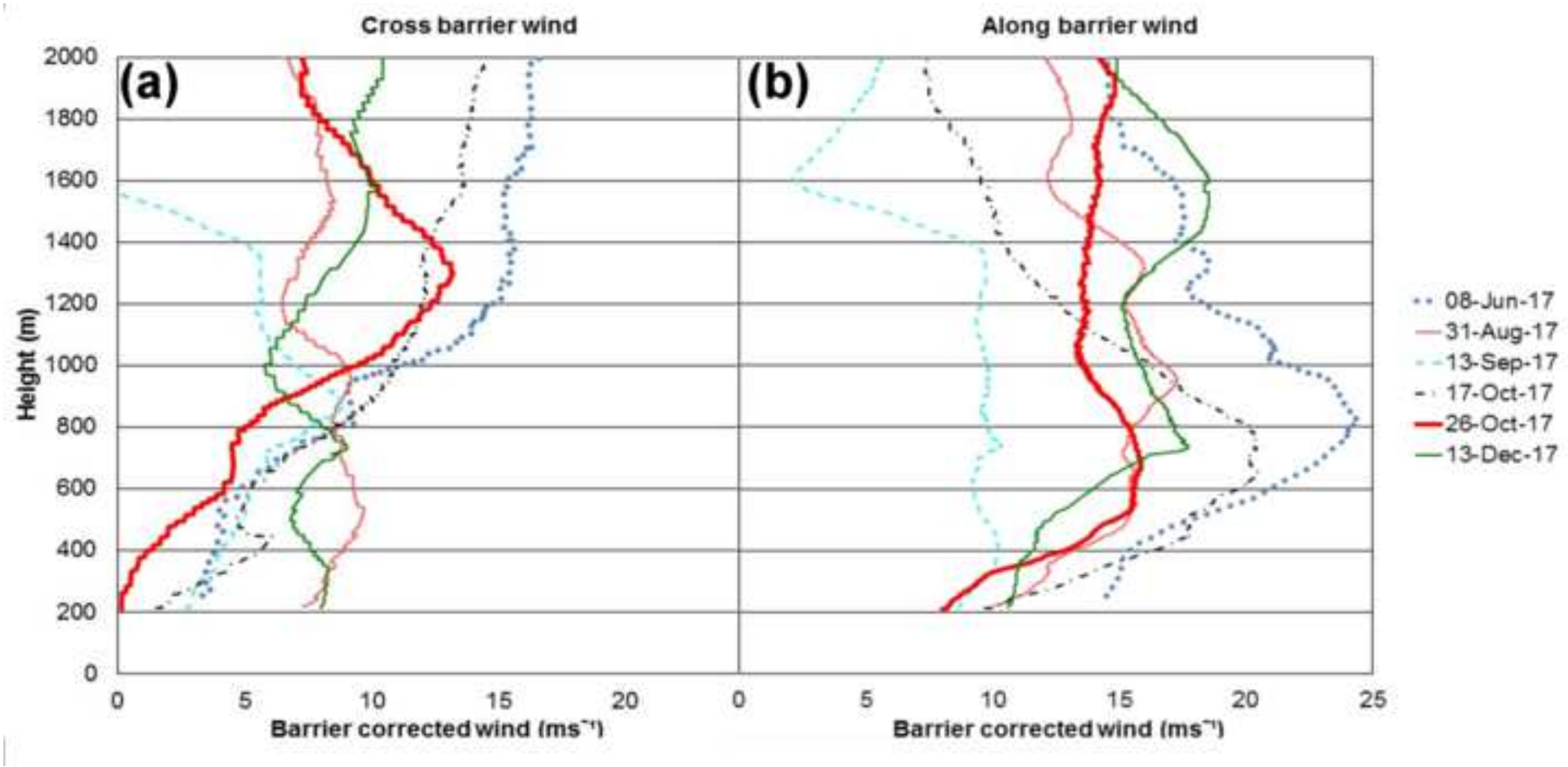
Cross barrier wind
Along barrier wind
(a)
(b)
Height (m)
2000
1800
1600
1400
1200
1000
800
600
400
200
0
0
5
10
15
20
25
Barrier corrected wind (ms¯¹)
08-Jun-17
31-Aug-17
13-Sep-17
17-Oct-17
26-Oct-17
13-Dec-17

Figure 7

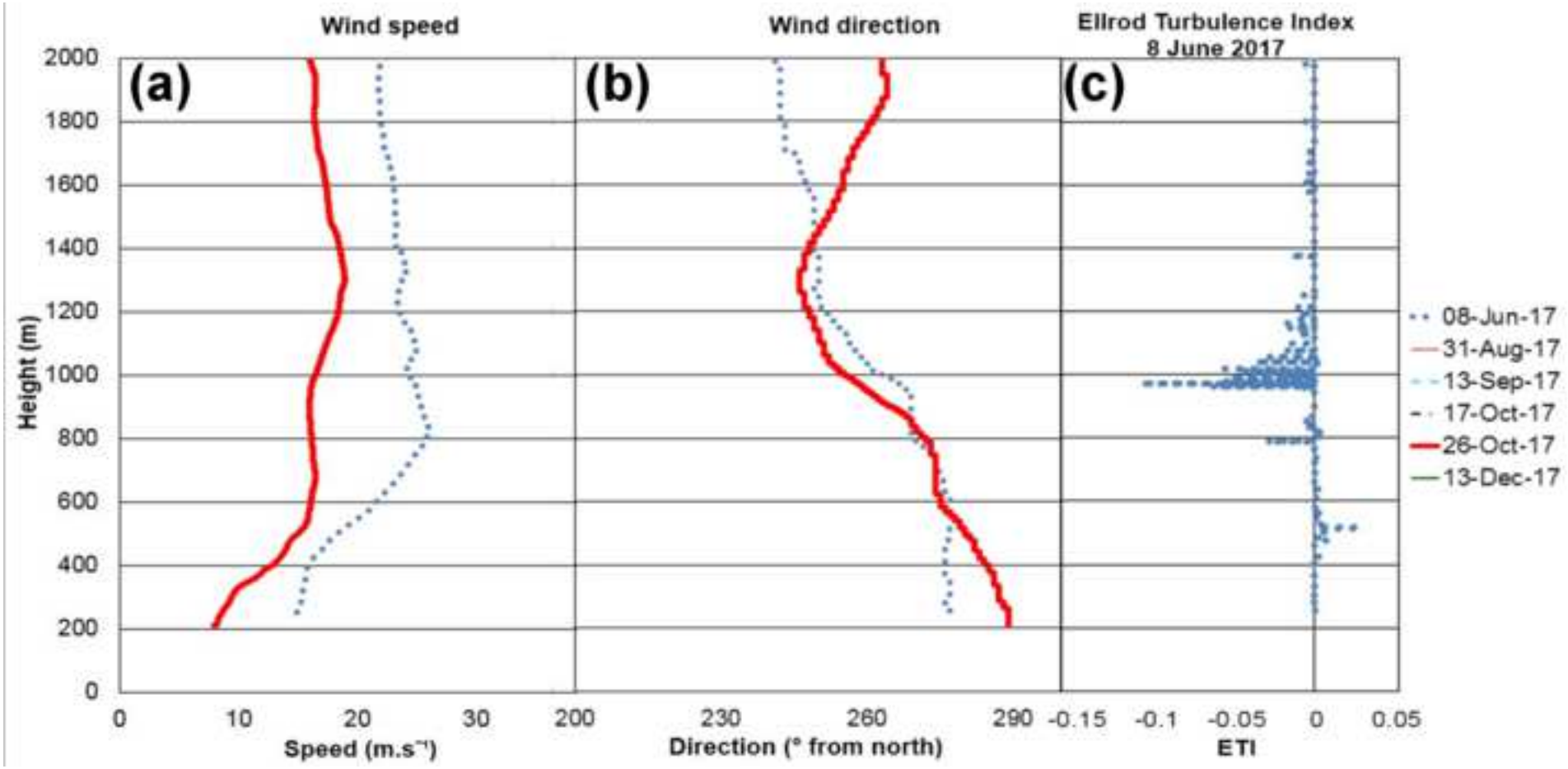
Wind speed
Wind direction
Ellrod Turbulence Index
8 June 2017
(a)
(b)
(c)
Height (m)
2000
1800
1600
1400
1200
1000
800
600
400
200
0
0
10
20
30
Speed (m.s⁻¹)
200
230
260
290
Direction (° from north)
-0.15
-0.1
-0.05
0
0.05
ETI
08-Jun-17
31-Aug-17
13-Sep-17
17-Oct-17
26-Oct-17
13-Dec-17

Figure 8

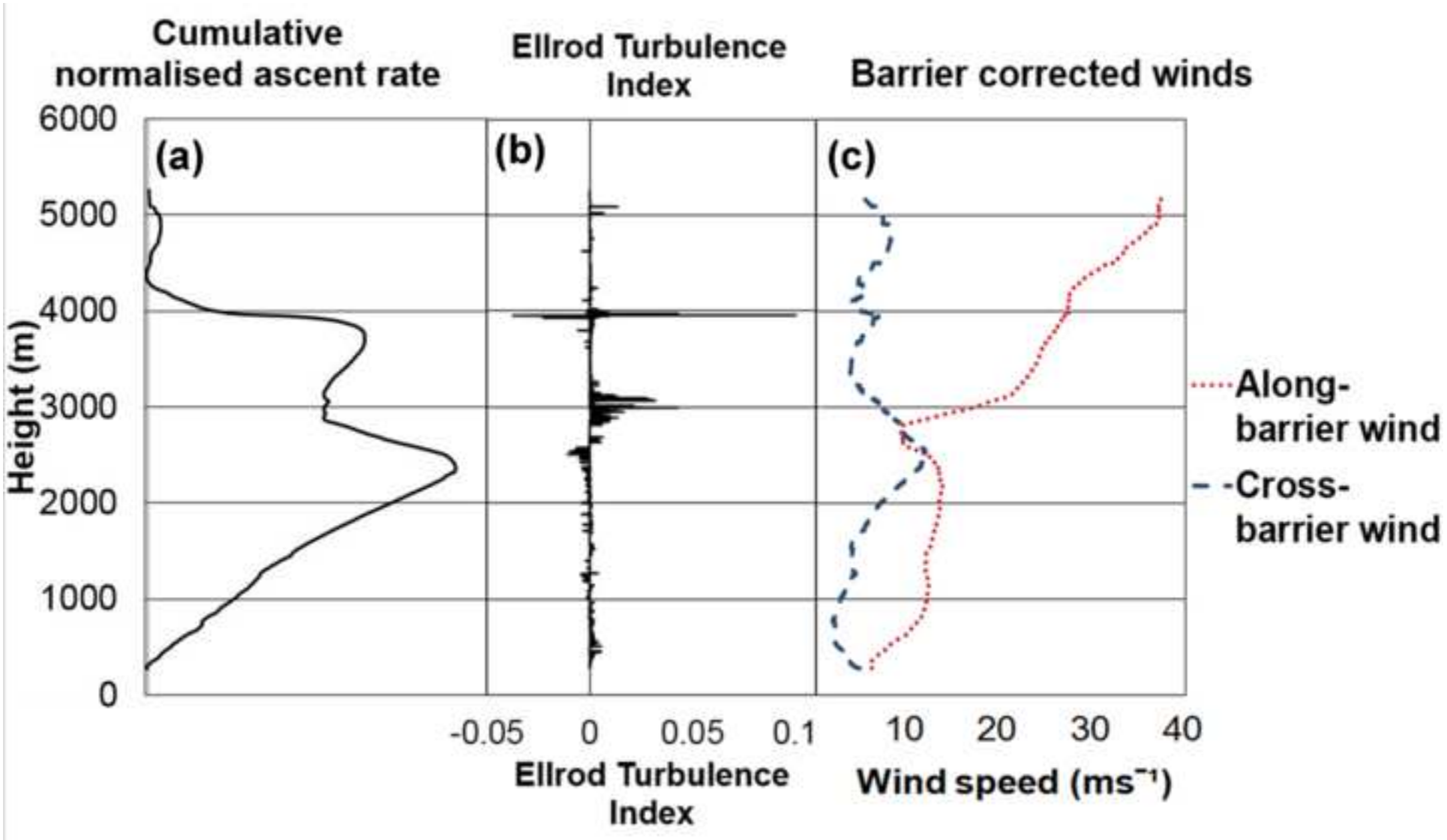
Cumulative normalised ascent rate
Ellrod Turbulence Index
Barrier corrected winds
(a)
(b)
(c)
Height (m)
6000
5000
4000
3000
2000
1000
0
-0.05
0
0.05
0.1
Ellrod Turbulence Index
10
20
30
40
Wind speed (ms⁻¹)
Along-barrier wind
Cross-barrier wind

Figure 9

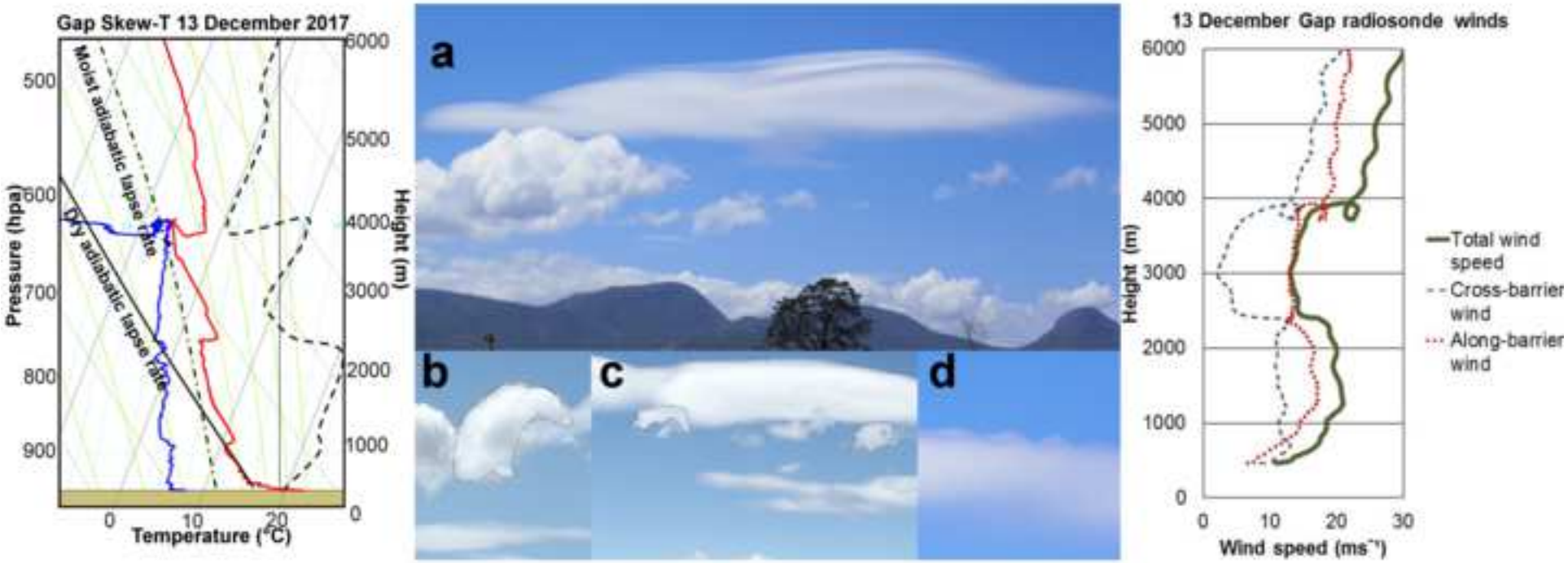
Gap Skew-T 13 December 2017
Moist adiabatic lapse rate
Dry adiabatic lapse rate
Pressure (hpa)
Height (m)
Temperature (°C)
a
b
c
d
13 December Gap radiosonde winds
Height (m)
Wind speed (ms⁻¹)
Total wind speed
Cross-barrier wind
Along-barrier wind